Computer Modeling in Engineering & Sciences

Tech Science Press

https://doi.org/10.32604/cmes.2026.082514

ARTICLE

Interpretable Seepage Discharge Forecasting in Earth-Rock Dams Using an Ensemble Model

Menghua Li[1,2,3], Bin Ou[1,2,3,4], Jiahao Li[1,2,3], Sitong Jin[1,2,3], Yanming Zhang[1,2,3] and Shuyan Fu[1,2,3,*]

[1]College of Water Conservancy, Yunnan Agricultural University, Kunming, China
[2]Yunnan Small and Medium-Sized Water Conservancy Project, Intelligent Management and Maintenance Engineering Research Center, Kunming, China
[3]Yunnan Key Laboratory of Water Security, Kunming, China
[4]State Key Laboratory of Water Disaster Prevention, Hohai University, Nanjing, China

*Corresponding Author: Shuyan Fu. Email: 2007004@ynau.edu.cn

Received: 17 March 2026; Accepted: 27 May 2026; Published: 30 June 2026

ABSTRACT: Accurate prediction of seepage discharge in earth-rock dams remains challenging due to the strong non-stationary and nonlinear characteristics, limited robustness of individual models, and poor interpretability of black-box approaches. To address these issues, this paper proposes an interpretable hybrid model that integrates Variational Mode Decomposition (VMD), Long Short-Term Memory (LSTM) networks, and Support Vector Machine (SVM). The model first decomposes the seepage discharge sequence and relevant lagged features using VMD. The LSTM network then captures temporal dependencies of the decomposed components, while the SVM performs regression on the original sequences and features. An adaptive fusion mechanism is established based on validation-set performance, using a 10% MAE-difference threshold selected from nearby candidate settings. Additionally, the SHapley Additive exPlanations (SHAP) framework is incorporated to quantify feature contributions. Experimental results demonstrate that the proposed model achieves MAE, root mean square error (RMSE), and mean absolute percentage error (MAPE) values of 0.0124 L/s, 0.0198 L/s, and 8.75%, respectively, outperforming the benchmark models, with R^2 improved to 0.9811. SHAP analysis further identifies reservoir water level as the most influential feature, contributing 37.5% to the predictions and showing broad consistency with engineering understanding of seepage behavior. By integrating VMD, LSTM, and SVM within an adaptive and interpretable workflow, this study enhances both predictive accuracy and interpretability, offering a reliable basis for anomaly diagnosis in earth-rock dam seepage monitoring.

KEYWORDS: Earth-rock dam; seepage discharge prediction; SHapley Additive exPlanations (SHAP); variational mode decomposition (VMD); long short-term memory (LSTM); support vector machine (SVM)

1 Introduction

Earth-rock dams serve as critical hydraulic infrastructure, fulfilling essential functions in global water resource management, flood protection, and energy supply. This dam type constitutes approximately 70% of the world's total dam inventory, and its structural safety directly affects public security and socioeconomic development [1]. Seepage, as a key indicator of dam structural behavior, is significantly correlated with dam failure events. Statistical evidence indicates that approximately 25% of dam failures are associated with seepage anomalies [2]. Consequently, achieving high-precision seepage discharge prediction not only enables early identification of potential safety hazards but also provides scientific foundations for dam health assessment and risk management strategy formulation [3,4].

The evolution of seepage prediction methodologies has progressed through multiple research paradigms, with each approach striving to overcome limitations of its predecessors. Physics-based numerical models grounded in Darcy's law and finite element analysis provide fundamental mechanistic understanding of seepage processes [5]. However, these deterministic approaches continue to face persistent challenges in addressing parameter uncertainty, computational complexity, and material heterogeneity characterization [6]. To compensate for these limitations, statistical methods have been widely adopted as computationally efficient alternatives, employing regression analysis and time series models to identify statistical patterns in seepage dynamics. Nevertheless, traditional statistical models exhibit notable constraints when confronting the inherent non-stationarity and strong nonlinearity characteristic of seepage systems [7].

These methodological deficiencies have catalyzed exploration of advanced data-driven techniques, particularly deep learning models that demonstrate exceptional capabilities in complex time series modeling. LSTM networks, leveraging their gating mechanisms, effectively capture long-term dependencies in temporal sequences and have exhibited significant accuracy improvements across multiple hydrological prediction applications [8]. Complementarily, SVM models have demonstrated robust performance in nonlinear regression tasks within geotechnical engineering contexts, maintaining strong generalization capability even under sample-limited conditions [9]. However, the isolated application of these machine learning approaches presents notable trade-offs: while LSTM excels at characterizing temporal patterns, it remains insufficient in capturing global feature interactions; conversely, although SVM provides robust regression capability, it inherently lacks explicit temporal dynamics modeling mechanisms [10].

Recent research has increasingly focused on integrating signal decomposition methods with machine learning to address the multi-scale and non-stationary characteristics inherent in seepage signals. Fatehi-Nobarian and Fard Moradinia demonstrated that models combining wavelet transform with artificial neural networks outperformed traditional ANN models in heterogeneous earth dam seepage prediction [11]. Liu et al. [12] further proposed an optimization framework integrating ICEEMDAN decomposition, multi-model ensemble, and adaptive weighting strategies, achieving significant improvements in both prediction stability and accuracy. Among signal decomposition techniques, VMD was introduced by Dragomiretskiy and Zosso. Rooted in a non-recursive variational optimization framework with a solid mathematical foundation, VMD demonstrates notable advantages in processing non-stationary signals [13]. VMD adaptively decomposes signals into band-limited intrinsic mode functions, effectively overcoming the mode mixing problem prevalent in empirical mode decomposition, and has demonstrated superior performance across diverse hydrological applications [14,15]. However, despite these advances, research on systematic integration of VMD with machine learning models remains preliminary, particularly in seepage prediction where a unified and reliable modeling framework has yet to be established.

While machine learning achieves favorable prediction accuracy in seepage applications, its "black-box" nature severely constrains credibility and practical deployment in safety-critical engineering contexts, with the primary obstacle being the lack of prediction interpretability. Traditional interpretability approaches, such as the random forest-based feature importance quantification employed by Li et al. [16], provide some insights into variable contributions but remain inadequate for capturing complex nonlinear interactions within seepage systems. Recent developments in Explainable Artificial Intelligence (XAI) offer novel pathways for enhancing machine learning model transparency. Among these, the SHAP method, grounded in cooperative game theory, provides consistent and theoretically rigorous quantification of each feature's contribution to prediction outputs [17]. The SHAP framework proposed by Lundberg and Lee [18] established theoretical foundations for interpreting complex machine learning models and has found applications in engineering monitoring domains. For instance, Yu et al. [19] constructed an IAO-XGBoost ensemble model,

utilizing SHAP methodology to reveal nonlinear influence mechanisms of variables including upstream-downstream water level differences, foundation permeability coefficients, and material zoning parameters on seepage behavior. Similarly, Hu and Su [20] applied SHAP analysis to Random Forest and XGBoost models in hydraulic structure deformation prediction, effectively identifying key variable contributions and providing interpretability support for data-driven models. Recent related work has also explored interpretable ensemble learning in dam safety applications. For example, Zhang et al. [21] developed a dyke-dam piping prediction model based on data augmentation and interpretable ensemble learning, and used SHAP analysis to reveal the dominant factors affecting piping risk. Although their study focused on piping occurrence rather than seepage discharge forecasting, it similarly highlights the importance of combining predictive performance with interpretability in dam safety assessment. These studies demonstrate that SHAP can significantly enhance the interpretability and physical plausibility of seepage prediction models through quantifying feature contributions and revealing decision mechanisms.

To address the above limitations, this study proposes an interpretable VMD-LSTM-SVM framework for seepage discharge forecasting. Given the strong non-stationarity, multi-scale fluctuations, and nonlinear temporal dependence of seepage discharge series, VMD is first used to decompose the preprocessed seepage sequence into multiple intrinsic mode functions and a residual component, thereby reducing mode mixing and facilitating feature extraction at different temporal scales. LSTM is then employed to learn the temporal dependencies and nonlinear evolution patterns of each decomposed component. In parallel, SVM performs direct regression on the original seepage-related input features, providing a stable global regression reference in the original feature space and complementing the component-wise temporal learning of LSTM under limited-sample conditions.

On this basis, a validation-driven adaptive fusion mechanism is introduced to combine or select the outputs of the VMD-LSTM and SVM branches according to their relative predictive performance, thereby improving robustness under varying prediction conditions. In addition, SHAP-based feature attribution is incorporated to quantify the effects of key variables and enhance model interpretability. The novelty of this work lies not in the isolated use of VMD, LSTM, SVM, or SHAP, but in their coordinated integration into a unified prediction workflow that combines multi-scale decomposition, component-wise temporal learning, direct feature-space regression, adaptive fusion, and interpretable analysis for seepage discharge forecasting.

2 Research Methods

This study develops a VMD-LSTM-SVM coupled model for seepage discharge prediction. The model is designed as a problem-oriented hybrid framework, in which VMD is used to decompose non-stationary seepage sequences into multi-scale components, LSTM is employed to capture the temporal dependencies of each component, and SVM is introduced as a complementary regression branch to enhance generalization performance and global feature-response modeling. The detailed algorithmic principles are described in the following subsections.

2.1 Variational Mode Decomposition

VMD is an adaptive signal processing method based on a variational optimization framework, which decomposes non-stationary signals into K Intrinsic Mode Functions (IMFs) and one residual component by solving a constrained optimization problem. Compared to Empirical Mode Decomposition (EMD), VMD offers two major advantages [22]: (1) it effectively avoids mode mixing through frequency-domain bandwidth constraints; (2) each IMF component possesses well-defined center frequencies and finite bandwidth characteristics. In this study, VMD is applied to seepage discharge time series and related features decomposition to extract multi-band characteristics, providing high-quality modal features for subsequent LSTM modeling,

thereby enhancing model prediction accuracy and interpretability. The core principle involves constructing a variational optimization problem to achieve precise frequency-domain decomposition of non-stationary signal $f(t)$ while ensuring complete signal reconstruction.

(1) The signal decomposition follows the expression:

$$f(t) = \sum_{k=1}^{K} u_k(t) + \mathrm{RES}(t) \tag{1}$$

where $u_k(t)$ represents the k-th IMF with center frequency ω_k and finite bandwidth, reflecting oscillation characteristics at specific temporal scales (e.g., high-frequency fluctuations or low-frequency trends); K denotes the number of decomposition modes, which was selected through comparative analysis of candidate values based on validation-set performance; and $\mathrm{RES}(t)$ represents the residual component retained after extracting the K band-limited IMFs. Together, the IMFs and $\mathrm{RES}(t)$ preserve the information required for complete signal reconstruction.

(2) Constrained variational optimization problem: VMD achieves decomposition by minimizing the total bandwidth of IMF components. The constrained variational problem is formulated as:

$$\min_{\{u_k\},\{\omega_k\}} \left\{ \sum_{k=1}^{K} \left\| \partial_t \left(\left(\delta(t) + \frac{\mathrm{j}}{\pi t} \right) * u_k(t) \right) \mathrm{e}^{-\mathrm{j}\omega_k t} \right\|_2^2 \right\} \tag{2}$$

Subject to:

$$\sum_{k=1}^{K} u_k(t) + \mathrm{RES}(t) = f(t) \tag{3}$$

where ∂_t is the time derivative operator, enforcing IMF smoothness; $\delta(t) + \mathrm{j}/(\pi t)$ is the Hilbert transform kernel for analytic signal construction; $\mathrm{e}^{-\mathrm{j}\omega_k t}$ shifts the IMF spectrum to baseband for bandwidth calculation.

2.2 Long Short-Term Memory Network

Following the VMD decomposition described in Section 2.1, which generates IMF components and residuals, LSTM models are employed to independently model the temporal dynamics of each component. LSTM is an enhanced Recurrent Neural Network (RNN) architecture [23], specifically designed to address gradient vanishing and exploding problems encountered by traditional RNNs when processing long sequence data. Compared to standard RNNs, LSTM dynamically regulates information flow through gating mechanisms—comprising input gates, forget gates, and output gates—thereby effectively modeling long-term dependencies in time series, making it an optimal architecture for temporal modeling tasks such as seepage discharge prediction.

The fundamental computational unit of LSTM consists of cell states and three gating structures. Through coordinated operation of these gating mechanisms, the architecture achieves efficient temporal data modeling, retaining critical historical information while adapting to dynamically changing input features. The specific structure is illustrated in Fig. 1.

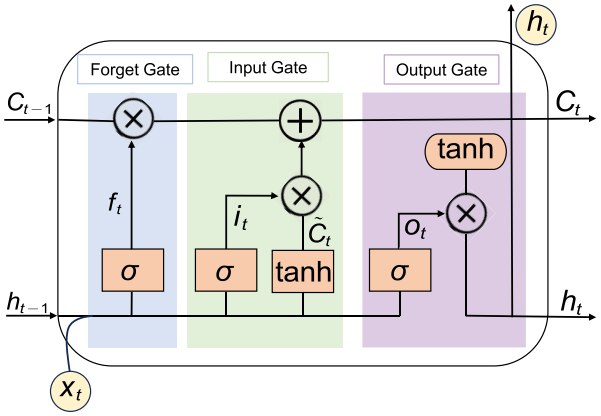

Figure 1: Internal structure of the LSTM unit.

In Fig. 1, C_{t-1} represents the previous cell state, while C_t denotes the updated cell state at the current time step. The model's computational process at time t follows these formulations:

- **Forget Gate:**

$$f_t = \sigma(W_f \cdot [h_{t-1}, x_t] + b_f) \tag{4}$$

where σ denotes the sigmoid activation function; W_f and b_f represent the forget gate's weight matrix and bias vector, respectively; h_{t-1} is the previous hidden state; x_t is the current input.

- **Input Gate:**

$$i_t = \sigma(W_i \cdot [h_{t-1}, x_t] + b_i) \tag{5}$$

$$\tilde{C}_t = \tanh(W_c \cdot [h_{t-1}, x_t] + b_c) \tag{6}$$

where i_t represents the input gate activation; $\tilde{C}_t$ denotes the candidate cell state; W_i is the input gate weight matrix; W_c represents the cell state weight matrix.

- **Cell State Update:**

$$C_t = f_t \cdot C_{t-1} + i_t \cdot \tilde{C}_t \tag{7}$$

- **Output Gate:**

$$o_t = \sigma(W_o \cdot [h_{t-1}, x_t] + b_o) \tag{8}$$

$$h_t = o_t \cdot \tanh(C_t) \tag{9}$$

where h_t represents the current hidden state, transmitted to the next time step; W_o denotes the output gate weight matrix.

In this study, each decomposed component generated by VMD was modeled using an independent LSTM branch with the same architecture and training settings. Specifically, a single-layer LSTM with 96 hidden units was adopted. Each input sample used a sequence length of 30 time steps. The hidden output sequence was further processed by a ReLU activation layer and a dropout layer with a dropout rate of 0.2, followed by a fully connected layer to generate a 7-dimensional output corresponding to the 7-day-ahead prediction horizon. The network was trained using the Adam optimizer with the mean squared error (MSE)

loss function. The initial learning rate, mini-batch size, and maximum number of epochs were set to 0.001, 70, and 70, respectively.

2.3 Support Vector Machine

Based on the preprocessed seepage discharge series, reservoir water level, and lagged feature data, the SVM branch performs direct regression in the original feature space. Unlike the VMD-LSTM branch, which focuses on learning component-wise temporal dependencies after decomposition, the SVM branch is used to retain the overall feature-response relationship among seepage discharge, reservoir water level, and lagged variables. In this way, it provides a stable complementary prediction for the hybrid framework under limited-sample conditions.

SVM, proposed by Vapnik et al. [24] and colleagues, is a supervised learning method grounded in statistical learning theory. Its core principle involves constructing optimal hyperplanes to achieve structural risk minimization, demonstrating unique advantages in addressing small-sample, nonlinear, and high-dimensional pattern recognition problems. Unlike traditional machine learning methods, SVM maps low-dimensional nonlinear problems into high-dimensional feature spaces through kernel functions, thereby obtaining global optimal solutions. This characteristic renders it particularly valuable for monitoring time series data analysis applications.

The application of SVM to regression problems is termed Support Vector Regression (SVR). The fundamental objective is to construct a function $f(x)$ that minimizes deviation between predicted and actual values while maintaining function smoothness. Given a training set $\{(x_i, y_i)\}_{i=1}^{n}$, where $x_i \in R$ represents input features and $y_i \in R$ denotes target outputs, the SVR objective function is defined as:

$$y = f(x) = w \cdot \phi(x) + b \tag{10}$$

where y represents the predicted value; w denotes the weight vector; b is the bias term; $\phi(x)$ represents the nonlinear mapping function transforming input data x from the original space to a high-dimensional feature space.

To determine optimal parameters w and b, SVR solves the following optimization problem:

$$\min_{w,b,\xi,\xi^*} \frac{1}{2}\|w\|^2 + C\sum_{i=1}^{n}(\xi_i + \xi_i^*) \tag{11}$$

$$s.t.\begin{cases} y_i - f(x_i) \le \epsilon + \xi_i \\ f(x_i) - y_i \le \epsilon + \xi_i^* \\ \xi_i, \xi_i^* \ge 0, i = 1, 2, \cdots, n \end{cases} \tag{12}$$

where $\|w\|^2$ represents the regularization term controlling model complexity; C denotes the penalty coefficient, representing the trade-off between model complexity and training error; ξ_i and ξ_i^* are slack variables permitting prediction deviations beyond the predefined tolerance range ϵ; ϵ defines the insensitive loss function parameter, specifying the error range excluded from loss calculation.

To efficiently solve this optimization problem, SVR introduces Lagrange multipliers a_i and a_i^*, transforming it into dual form, yielding the final decision function:

$$f(x) = \sum_{i=1}^{n}(a_i - a_i^*)K(x_i, x) + b \tag{13}$$

where $K(x_i, x)$ represents the kernel function computing inner products in the high-dimensional feature space.

In this study, a linear kernel function, $K(x_i, x_j) = x_i \cdot x_j$ is adopted for the SVM branch because it provides a parsimonious and computationally efficient formulation and shows stable generalization performance for the current dataset. Compared with the RBF kernel, which is more sensitive to local feature variations, and the polynomial kernel, which tends to fit more complex global patterns, the linear kernel yielded more stable validation results and reduced the risk of overfitting. Unlike the VMD-based LSTM branch, which predicts seepage discharge by learning the temporal evolution of decomposed components, the SVM branch directly models the relationship between seepage discharge and the original input variables in the feature space. This direct-regression strategy helps retain the overall influence of reservoir water level and lagged variables on seepage discharge. Therefore, SVM complements LSTM from a different modeling perspective: LSTM emphasizes temporal dynamics after decomposition, whereas SVM provides a stable global regression reference in the original feature space. The combination of these two branches helps improve both prediction robustness and overall accuracy.

2.4 SHAP Model Interpretation Method

This study adopts the SHAP method to provide interpretability analysis for the seepage discharge prediction model constructed using VMD, LSTM, and SVM. By quantifying each input feature's contribution to seepage discharge predictions, SHAP reveals the key features underlying model decision processes.

In earth-rock dam safety monitoring, model interpretability is crucial for accurately understanding the factors influencing seepage discharge variations. The SHAP method, grounded in game theory, calculates each feature's marginal contribution across all possible feature combinations (Shapley values), decomposing model prediction $f(x)$ into the additive contributions of n features. This approach quantitatively evaluates input feature impacts on seepage discharge predictions. The core calculation formula is:

$$\varphi_j = \sum_{S \subseteq N \setminus \{j\}} \frac{|S|(n - |S| - 1)!}{n!} [f(S \cup \{j\}) - f(S)] \tag{14}$$

where φ_j represents feature j's SHAP value; N denotes the set of all features; S represents a feature subset excluding feature j; $|S|$ indicates the subset size; n is the total number of features; $f(S \cup \{j\}) - f(S)$ represents the marginal contribution when feature j joins subset S; $|S|(n - |S| - 1)!/n!$ serves as the weighting coefficient reflecting the probability of feature combinations.

SHAP assumes that model predictions can be decomposed into the sum of individual feature contributions:

$$f(x) = \varphi_0 + \varphi_1 + \varphi_2 + \cdots + \varphi_n \tag{15}$$

where $f(x)$ represents the model's prediction for a specific sample; φ_0 denotes the baseline value (typically the dataset's average prediction); φ_i (i = 1, . . ., n) represents the i-th feature's SHAP value, indicating its contribution to the prediction.

2.5 Coupled Model Construction

Based on the above methodological design, a coupled VMD-LSTM-SVM framework was constructed for seepage discharge forecasting, as illustrated in Fig. 2. The workflow consists of data preprocessing and lag-feature construction, VMD-based signal decomposition, parallel prediction by the VMD-LSTM and SVM branches, validation-driven output integration, and SHAP-based interpretation. Through this procedure, the

framework combines component-wise temporal learning with direct feature-space regression to improve the accuracy, robustness, and interpretability of seepage discharge prediction.

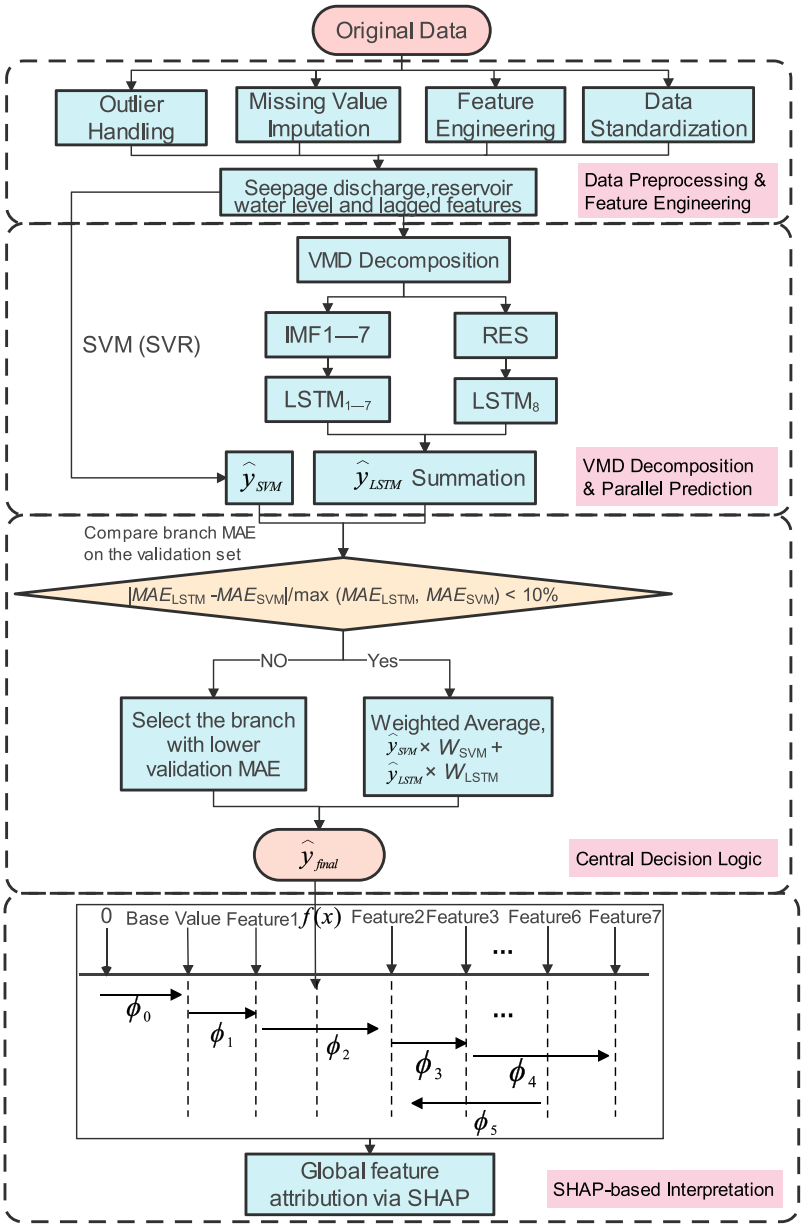

Figure 2: Interpretable seepage discharge prediction workflow of the ensemble model.

The model construction and prediction process comprises the following steps:

Step1: Data Preprocessing

For seepage discharge prediction, comprehensive preprocessing was performed on the dataset containing date, reservoir water level, and seepage discharge measurements. The dataset was first sorted and partitioned in strict chronological order, without random shuffling, to preserve the temporal structure of the time series and avoid information leakage during model development. First, the interquartile range

method was used to identify outliers, and no significant anomalies were found in the water-level and seepage-discharge series. For the 106 missing values in the seepage discharge series, cubic spline interpolation was applied, with forward and backward filling used for the endpoints where needed.

Within this chronological framework, lagged features were constructed by shifting the reservoir water level and seepage discharge series by 1, 2, and 3 days, yielding water_level_lag_1, water_level_lag_2, water_level_lag_3, seepage_lag_1, seepage_lag_2, and seepage_lag_3. Together with the current reservoir water level, these variables formed the input feature set, while seepage discharge was used as the prediction target. The date field was used only for chronological ordering and was not directly used as a predictor. The 1–3 day lag settings were selected to capture the short-term delayed response of seepage to recent hydraulic conditions while avoiding unnecessary feature redundancy and excessive model complexity. Before model training, the numerical input features were normalized to the [0,1] interval using Min-MaxScaler, with scaling parameters fitted on the training set only and then applied to the validation and test sets.

These preprocessing operations were designed to mitigate the influence of measurement uncertainty, missing observations, and data irregularities before model training. No additional signal-smoothing filter was applied in this study, so as to avoid suppressing physically meaningful short-term seepage fluctuations. Instead, data quality control was achieved through outlier screening, missing-value imputation, lag-feature construction, and feature normalization, while the subsequent VMD step further helped separate high-frequency disturbances from the main seepage signal.

Step2: Data Decomposition

The VMD algorithm decomposes the original seepage discharge time series into multiple IMFs and one residual component. During decomposition, modal quantities and bandwidth parameters are determined by optimizing the constrained variational problem, ensuring accuracy and physical meaningfulness of decomposition results.

Step3: LSTM Modeling

Individual LSTM models are constructed for each IMF and residual component. Through input, forget, and output gate mechanisms, LSTM learns the temporal dependencies of each component and generates corresponding prediction sequences.

Step4: SVM Prediction

All LSTM branch predictions are aggregated to obtain a preliminary seepage discharge prediction that primarily reflects the temporal evolution patterns learned from the VMD-decomposed components. In parallel, SVM constructs a direct regression model based on the original feature set and generates an independent prediction. Therefore, the two branches provide complementary information: the LSTM branch emphasizes decomposed temporal dynamics, whereas the SVM branch preserves the overall feature–response relationship in the original feature space.

Step5: Results Integration

A dynamic weighted ensemble strategy integrates the predictions from the VMD-LSTM branch and the SVM branch. Specifically, both branches are first evaluated on the validation set using MAE. In this study, a 10% relative MAE-difference threshold was selected after comparing nearby candidate settings, as it provided the most balanced validation performance while preserving stable final prediction accuracy. This threshold is used to distinguish cases in which the two branches show comparable predictive performance from cases in which one branch has a clear validation advantage. Let MAE_{LSTM} and MAE_{SVM} denote the validation-set MAE values of the VMD-LSTM branch and the SVM branch, respectively. Let $\hat{y}_{\mathrm{LSTM}}$ denote the aggregated prediction from the VMD-LSTM branch, $\hat{y}_{\mathrm{SVM}}$ denote the prediction generated by the SVM

branch, and $\hat{y}_{\text{final}}$ denote the final ensemble prediction. Based on this criterion, the following ensemble rules are established:

Rule 1: When

$$\frac{|MAE_{\text{LSTM}} - MAE_{\text{SVM}}|}{\max\left(MAE_{\text{LSTM}}, MAE_{\text{SVM}}\right)} < 10\%$$

the performance gap is considered small, and weighted fusion is applied to retain complementary information from both branches. In this case, inverse-error weights are used:

$$w_{\text{LSTM}} = \frac{1/MAE_{\text{LSTM}}}{1/MAE_{\text{LSTM}} + 1/MAE_{\text{SVM}}} \tag{16}$$

$$w_{\text{SVM}} = \frac{1/MAE_{\text{SVM}}}{1/MAE_{\text{LSTM}} + 1/MAE_{\text{SVM}}} \tag{17}$$

and the final prediction is obtained as

$$\hat{y}_{\text{final}} = w_{\text{LSTM}}\hat{y}_{\text{LSTM}} + w_{\text{SVM}}\hat{y}_{\text{SVM}} \tag{18}$$

so that the branch with the lower validation MAE receives the larger fusion weight.

Rule 2: When

$$\frac{|MAE_{\text{LSTM}} - MAE_{\text{SVM}}|}{\max\left(MAE_{\text{LSTM}}, MAE_{\text{SVM}}\right)} \geq 10\%$$

one branch is considered to have a clear validation advantage, and the better-performing branch is directly selected to avoid introducing additional error from the weaker branch. Thus,

$$\hat{y}_{\text{final}} = \begin{cases} \hat{y}_{\text{LSTM}}, & MAE_{\text{LSTM}} < MAE_{\text{SVM}}, \\ \hat{y}_{\text{SVM}}, & MAE_{\text{SVM}} < MAE_{\text{LSTM}}. \end{cases}$$

This ensemble strategy effectively combines the component-wise temporal learning capability of LSTM with the stable direct-regression capability of SVM. By retaining complementary information when the two branches exhibit comparable validation performance and favoring the better-performing branch when the validation gap becomes sufficiently large, it integrates decomposed dynamic information with original feature-space relationships to enhance seepage discharge prediction accuracy and robustness.

Step6: Model Evaluation

Multi-dimensional metrics comprehensively assess the VMD-LSTM-SVM ensemble model performance, including MAE, MSE, RMSE, MAPE and R^2. Through comprehensive analysis of these metrics, the model's performance across training, validation, and test sets is systematically examined, providing quantitative evidence for validating the ensemble model's superiority over the benchmark models.

Step7: Result Interpretation

To enhance model interpretability, a SHAP-based analysis is introduced for the VMD-LSTM-SVM framework. Deep SHAP is used to interpret the VMD-LSTM branch, and Kernel SHAP is used to interpret the SVM branch. For the final ensemble output, the branch-level SHAP values are combined according to the same decision logic as that used for prediction: when the two branches are fused, the final SHAP values are obtained through weight-consistent integration of the two branch-level explanations; when one

branch is directly selected as the final predictor, the SHAP explanation of that selected branch is used as the final interpretation. This strategy ensures consistency between the prediction mechanism and the interpretation process.

3 Engineering Case Study

This study employs seepage monitoring data from an earth-rock dam in Yunnan Province, China, to validate the predictive performance of the VMD-LSTM-SVM model. The selected dam is a large Type-II earth-rock dam with clear seepage–water-level response characteristics, making it a suitable engineering case for methodological verification. Seven input features were used, including the current reservoir water level, three lagged reservoir water level terms (water_level_lag_1 to water_level_lag_3), and three lagged seepage terms (seepage_lag_1 to seepage_lag_3). The dataset was divided into training, validation, and test sets at a ratio of 7:1:2, and the predictive effectiveness of the proposed framework was evaluated by comparison with two simpler single-model baselines (LSTM and SVM) and two intermediate hybrid comparison models (LSTM-SVM and VMD-LSTM). The present work was designed as a single case study to examine the feasibility and predictive capability of the proposed framework under a real engineering scenario, while broader applicability should be further validated on multiple dams.

3.1 Project Overview

The study focuses on a large Type-II earth-rock dam project in Kunming, Yunnan Province. The main dam features a crest length of 201 m, maximum height of 62 m, crest elevation of 1976 m, normal water storage level of 1965.5 m, and total reservoir capacity of 229 million m^3. Five seepage monitoring points (designated ZU1-ZU5) are installed along the main dam's riverbed section, with a triangular measuring weir positioned at the downstream toe (location details shown in Fig. 3) for continuous seepage discharge monitoring.

Figure 3: Location plan of seepage monitoring points and the gauge weir on the main dam.

Monitoring data indicate that during the operational period from 1 January 2010, to 24 September 2012, the main-dam seepage discharge varied between 5.61–11.48 L/s. Fig. 4 illustrates the temporal variation characteristics of seepage discharge, rainfall, and reservoir water level monitoring data. Results demonstrate

no direct correlation between seepage discharge trends and rainfall fluctuations, indicating that the measuring weir effectively isolates surface runoff interference, allowing seepage measurements to accurately reflect dam seepage conditions. The reservoir water level and seepage discharge data employed in this study originate from this monitoring period (see Fig. 4), exhibiting lagged response relationships consistent with fundamental Darcy flow theory.

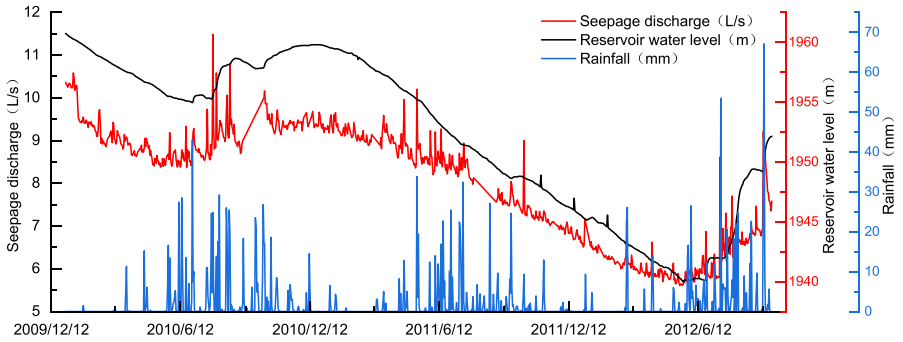

Figure 4: Time series plot of seepage discharge, reservoir water level, and rainfall.

3.2 Model Analysis

This study utilizes 998 daily seepage discharge and reservoir water level observations from the monitoring period to validate the proposed VMD-LSTM-SVM framework. The dataset was partitioned in strict chronological order, without random shuffling, into training (698 samples), validation (100 samples), and test (200 samples) subsets at a ratio of 7:1:2. Based on this fixed split, an additional 7-day-ahead seepage discharge prediction experiment was conducted on the held-out test set, using the trained model without rolling re-training or walk-forward updating. To comprehensively evaluate the proposed framework, four representative benchmarks were adopted: two standalone baselines (LSTM and SVM) and two partial hybrid baselines (VMD-LSTM and LSTM-SVM). This benchmark design enables a stepwise assessment of the contributions of signal decomposition, temporal modeling, direct regression, and their adaptive integration within the full VMD-LSTM-SVM framework. Table 1 summarizes the parameter configurations for the VMD, LSTM, and SVM modules.

The number of modes K is a key parameter in VMD, as it directly affects the decomposition granularity and the subsequent prediction performance. In this study, candidate values of $K = 6$, 7, and 8 were comparatively evaluated. These values were chosen to represent a reasonable range around the expected decomposition complexity of the seepage discharge series, so as to avoid both under-decomposition and over-decomposition. The final value of K was selected according to the prediction performance on the validation set. Among the tested candidates, $K = 7$ yielded the most balanced decomposition and the best validation performance, and was therefore adopted in the subsequent analysis.

For the SVM branch, a linear kernel function was adopted because it provided a parsimonious and computationally efficient formulation with stable generalization performance for the current dataset. Compared with the RBF kernel, which is more sensitive to local feature variations, and the polynomial kernel, which tends to fit more complex global patterns, the linear kernel produced more stable validation results and reduced the risk of overfitting. This choice should not be interpreted as implying that the overall seepage prediction problem is fully linear; rather, the linear-kernel SVM serves as a complementary regression branch in the original feature space, while the non-stationary and multi-scale temporal characteristics are mainly addressed by the VMD and LSTM components.

Table 1: Configuration of parameters for the VMD-LSTM-SVM model.

Module	Parameter	Value
VMD	K	7
	α	2000
LSTM	Sequence length	30
	Number of LSTM layers	1
	Hidden units	96
	Dropout rate	0.2
	Output dimension	7
	Optimizer	Adam
	Loss function	MSE
	Mini-batch size	70
	Epochs	70
	Initial learning rate	0.001
SVM	Kernel function	linear
	Scale	1
	Regularization parameter (C)	1

3.2.1 VMD Decomposition of Seepage Discharge Time Series

Considering the non-stationary and multi-scale characteristics of seepage data, this study applied VMD to decompose the preprocessed seepage discharge and lagged feature data. As noted above, candidate values of K = 6, 7, and 8 were comparatively evaluated, and K = 7 was selected based on validation-set performance together with the balance and interpretability of the decomposition results. The corresponding decomposition results are presented in Fig. 5. For visualization purposes, the VMD components shown in Fig. 5 were concatenated in chronological order after partition-wise processing of the training, validation, and test subsets; this visualization does not affect the chronological data-splitting protocol used for modeling.

As shown in Fig. 5, VMD decomposes the seepage discharge series into seven intrinsic mode functions (IMF1–IMF7) and one residual component (RES). IMF1–IMF4 are high-frequency components with relatively small amplitudes, mainly characterizing short-term fluctuations. IMF5 exhibits intermediate-frequency oscillations, indicating periodic or episodic variations. IMF6 reflects lower-frequency variability and captures slower medium-term undulations. IMF7 is the lowest-frequency component and represents the baseline level and long-term evolution of seepage discharge. By contrast, the RES component remains close to zero mean and has relatively small amplitude, indicating that only limited residual information remains after the dominant multi-scale oscillatory and trend characteristics have been extracted. Although its magnitude is relatively small, RES is still retained as an independent component in the subsequent modeling stage to preserve complete signal information.

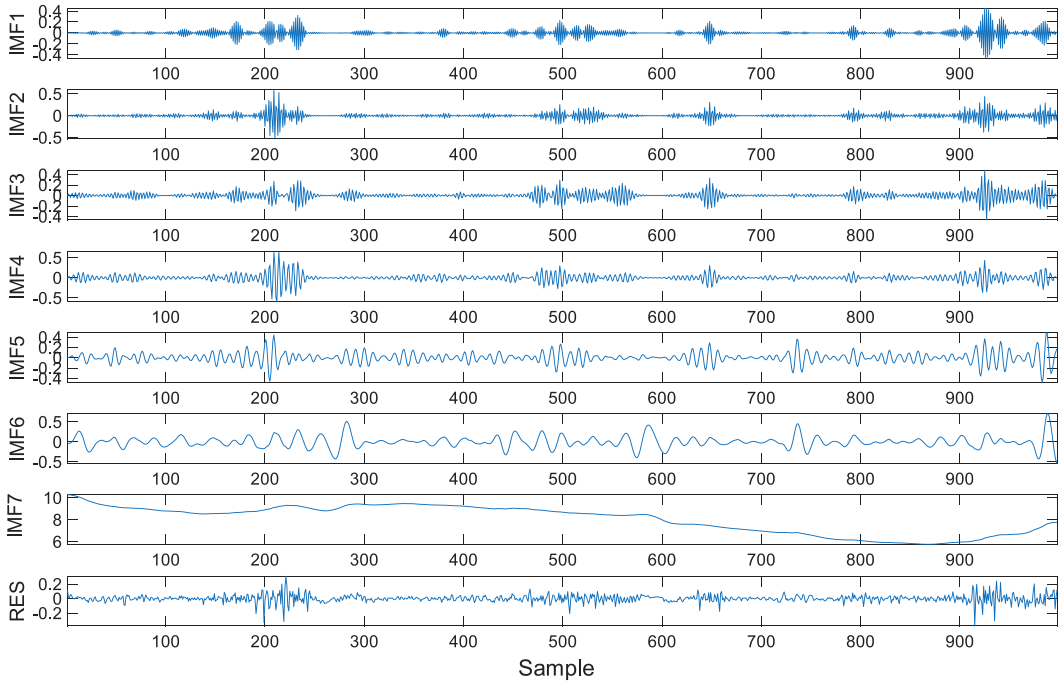

Figure 5: Decomposition results of VMD.

According to Eq. (1), the original seepage discharge series $f(t)$ can be reconstructed by summing all decomposed components, i.e.,

$$\hat{f}(t) = \sum_{k=1}^{K} u_k(t) + \mathrm{RES}(t) \tag{19}$$

To verify that the selected VMD decomposition preserves the original signal information, the reconstructed series $\hat{f}(t)$ was compared with the original series $f(t)$, and the reconstruction error was defined as

$$e(t) = f(t) - \hat{f}(t) \tag{20}$$

As shown in Fig. 6, the reconstructed series almost completely overlaps with the original seepage discharge series, while the reconstruction error remains near zero throughout the entire period, with only negligible numerical deviations at the numerical precision level. Specifically, panel A in Fig. 6 compares the original seepage discharge series $f(t)$ with the reconstructed series $\hat{f}(t)$, whereas panel B presents the reconstruction error series $e(t) = f(t) - \hat{f}(t)$. These results confirm that the selected VMD decomposition achieves accurate signal reconstruction and provides a reliable basis for the subsequent component-wise prediction modeling.

3.2.2 VMD-LSTM-SVM Model Seepage Discharge Prediction Analysis

The previous section demonstrated how VMD decomposes seepage discharge, reservoir water level, and lagged feature data into IMF1–IMF7 and RES, each reflecting distinct frequency characteristics. These components serve as inputs to LSTM for prediction. Eight independent LSTM models [25] were constructed for IMF1–IMF7 and the residual component. All eight LSTM branches employed the same network architecture and training hyperparameters, and differed only in the decomposed input components

assigned to each branch. Each LSTM model receives its corresponding component and related features (such as water-level lag terms), learning temporal patterns within each component—including short-term fluctuations and periodic trends—through input, forget, and output gate mechanisms. LSTM updates hidden states sequentially through time steps, generating prediction sequences, with all component predictions subsequently aggregated to produce preliminary seepage discharge predictions. Concurrently, the SVM branch performs regression based on the original seepage-related input features, utilizing a linear kernel function to construct a stable global regression model in the original feature space. While the LSTM branch focuses on learning temporal patterns within decomposed components, the SVM branch provides an independent prediction that retains the overall influence of reservoir water level and lagged variables. In this way, SVM offers a complementary prediction perspective and helps compensate for the limitations of relying only on component-wise temporal modeling.

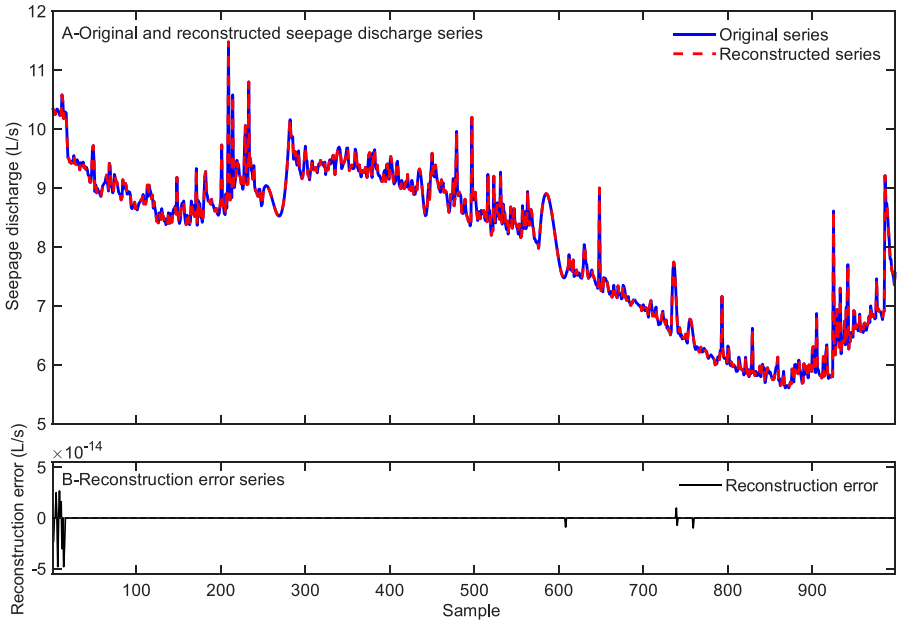

Figure 6: Reconstruction validation of the VMD decomposition.

The validation-set MAE was calculated separately for the aggregated VMD-LSTM branch and the SVM branch. When the relative MAE difference was below 10%, the two branches were considered to have comparable validation performance, and the final prediction was obtained by inverse-error weighted fusion. When the relative difference was 10% or greater, the branch with the lower validation MAE was directly selected, indicating a clear validation advantage (see Section 2.5 for details). The prediction horizon was set to 7 days. During test-time evaluation, 7-day-ahead predictions were generated on the fixed held-out test set using the trained model, without rolling re-training or walk-forward updating. This fixed test-setting was used to provide a controlled evaluation of model generalization, whereas practical deployment would require continuously updated monitoring inputs and periodic model recalibration or retraining. Fig. 7 shows the fitting performance on the training and test sets, Fig. 8 presents the corresponding seven-day-ahead prediction results.

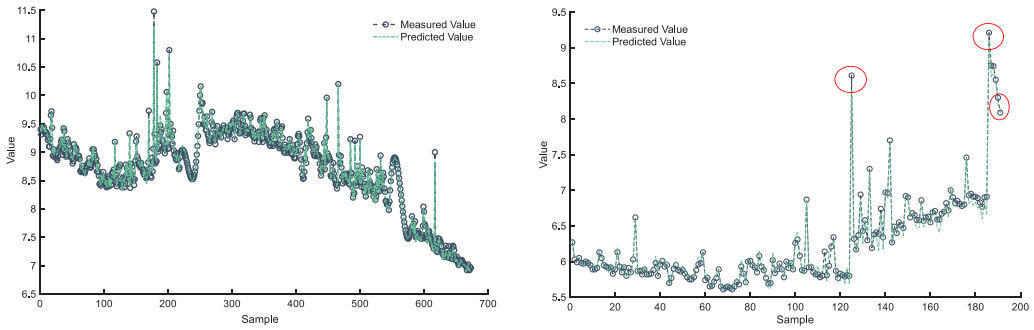

A Training Set Performance **B** Test Set Performance

Figure 7: Training-set and test-set fitting performance of the VMD-LSTM-SVM model.

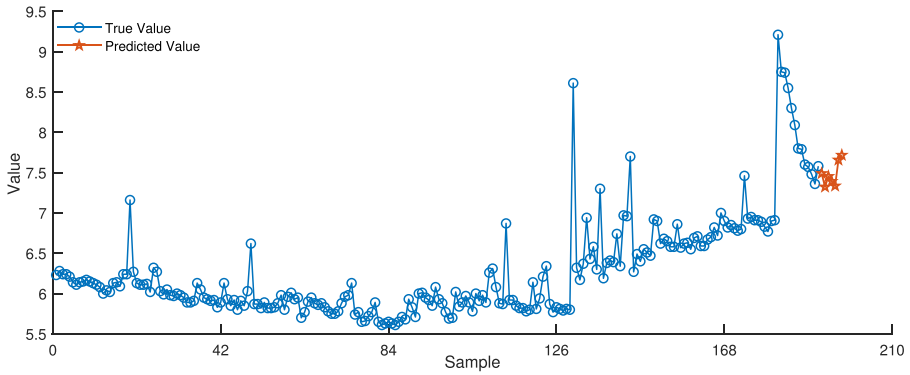

Figure 8: Seven-day-ahead prediction results of the VMD-LSTM-SVM model.

As shown in Fig. 7, the green curve (predicted) closely follows the gray curve with markers (measured) and reproduces both the fluctuation patterns and the baseline evolution of seepage discharge. In the training-set panel, values mainly lie within 7–11 with a gentle downward trend superimposed by periodic undulations; the model tracks peaks and troughs well, with only slight underestimation at a few sharp spikes. In the test-set panel, values are mostly in the 6–9.5 range, with a slowly rising baseline and several abrupt surges. Errors are generally small, but around 130–140, 175–185, and 195–200 the predictions are smoother and slightly lag the sharp peaks, leading to underestimation of these abrupt changes. Overall, the VMD-based dynamic weighted ensemble (VMD–LSTM–SVM) performs robustly on steady and moderate-variance segments, while there remains room to improve the depiction of high-frequency transients and extremes.

To comprehensively evaluate the proposed VMD-LSTM-SVM dynamic weighted ensemble model's performance in seepage discharge prediction, we calculated key metrics across training, validation, and test sets, including the mean absolute error (MAE), mean squared error (MSE), root mean squared error (RMSE), mean absolute percentage error (MAPE), and coefficient of determination (R^2) [26]. These metrics quantify prediction accuracy and reveal generalization capability across different datasets. Table 2 presents detailed metric values for each dataset.

Table 2: Prediction performance of the VMD-LSTM-SVM model across datasets.

Data Set	$MAE/(L/s)$	$MSE/(L/s)^2$	$RMSE/(L/s)$	R^2	$MAPE/\%$
Training Set	0.0075	0.0001	0.0122	0.9948	1.48
Validation Set	0.0080	0.0001	0.0105	0.9834	6.32
Test Set	0.0124	0.0004	0.0198	0.9811	8.75

Note: Refer to the density plot in Fig. 9 for the error distribution of the training and test sets.

Table 2 and Fig. 9 collectively demonstrate the VMD-LSTM-SVM model's performance in seepage discharge prediction. Table 2 reveals excellent performance on the training set, with R^2 of 0.9948 and MAE of merely 0.0075 L/s, indicating extremely high prediction accuracy. On the test set, R^2 reaches 0.9811 with MAE increasing to 0.0124 L/s and MAPE of 8.75%, showing some decline in generalization capability. Fig. 9 presents density scatter plots with regression lines for both training and test set predictions vs. actual values. Training set points cluster tightly around the regression line ($y = 1.017x - 0.142$), demonstrating high concordance between predicted and actual values, consistent with the R^2 of 0.9948 in Table 2. Test set points exhibit slightly greater dispersion but remain predominantly concentrated near the regression line ($y = 0.794x + 1.454$), with R^2 of 0.9811, indicating reliable predictive capability on new data. The degree of scatter deviation from the regression line intuitively reflects model fitting quality: training set points are more concentrated with higher prediction accuracy, while test set points show greater dispersion with slightly larger errors, corresponding to the elevated MAE values in Table 2.

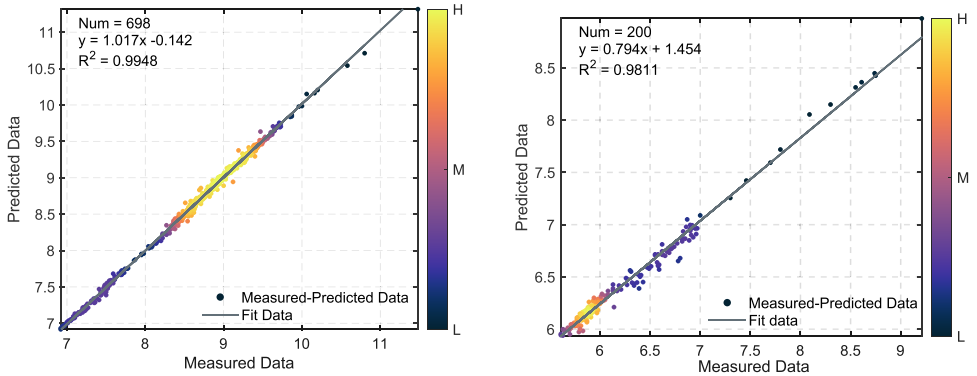

A Training Set Density Plot **B** Test Set Density Plot

Figure 9: Density plots of predicted vs. measured seepage discharge for the training set and test set.

To further evaluate the robustness of the threshold used in the adaptive fusion strategy, additional comparisons were conducted with nearby MAE-difference thresholds of 5%, 10%, and 15%, as summarized in Table 3. The results show that the overall prediction performance remains broadly stable across these nearby settings, indicating that the final results are not overly sensitive to modest threshold variations. Among them, the 10% threshold yields the best validation performance and also provides the best overall test performance. Therefore, 10% was retained as the final threshold in this study.

To further validate the proposed VMD-LSTM-SVM ensemble model's predictive capability, quantitative analysis systematically compares it with VMD-LSTM, LSTM-SVM, LSTM, and SVM models. Evaluation employs multiple key performance metrics including MAE, MSE, RMSE, MAPE, and R^2 to comprehensively assess prediction accuracy and stability. Fig. 10 presents a radar chart visually illustrating performance differences across these dimensions, providing clear comparative insights into model strengths and weaknesses.

The VMD-LSTM-SVM model achieves test-set MAE of 0.0124 L/s, MSE of 0.0004 $(L/s)^2$, RMSE of 0.0198 L/s, MAPE of 8.75%, and R^2 of 0.9811, demonstrating the best overall performance.

Table 3: Sensitivity comparison of nearby MAE-difference thresholds in the adaptive fusion strategy.

Threshold	Validation Set			Test Set		
	MAE (L/s)	RMSE (L/s)	R^2	MAE (L/s)	RMSE (L/s)	R^2
5%	0.0083	0.0109	0.9828	0.0128	0.0203	0.9803
10%	0.0080	0.0105	0.9834	0.0124	0.0198	0.9811
15%	0.0082	0.0107	0.9830	0.0126	0.0201	0.9807

Note: Only validation-set and test-set metrics are reported here for brevity, as the threshold selection is based on validation performance and its influence is mainly evaluated through final predictive performance.

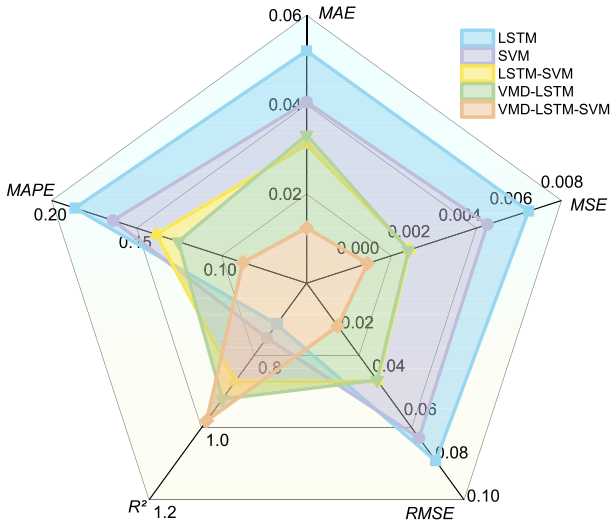

Figure 10: Radar chart comparing evaluation metrics of different models.

Compared with the two simpler single-model baselines, LSTM and SVM, the proposed model shows substantial improvement. Relative to LSTM, MAE, RMSE, and MAPE are reduced by 76.19%, 75.81%, and 53.03%, respectively, while R^2 increases from 0.7139 to 0.9811. Relative to SVM, MAE, RMSE, and MAPE are reduced by 69.48%, 72.24%, and 46.61%, respectively, with R^2 increasing from 0.7515 to 0.9811. The proposed model also outperforms the two intermediate hybrid comparison models. Compared with VMD-LSTM, it reduces MAE by 62.65%, MSE by 80.00%, RMSE by 55.70%, and MAPE by 30.22%, while improving R^2 by 6.57%. Relative to LSTM-SVM, it achieves MAE, MSE, RMSE, and MAPE reductions of 60.00%, 80.00%, 56.19%, and 36.82%, respectively, together with a R^2 improvement of 12.54%. These stepwise comparisons indicate that the superiority of the proposed framework is not attributable to a direct stacking of existing modules. Rather, the performance gain arises from the coordinated integration of multi-scale decomposition, component-wise temporal learning, direct feature-space regression, and adaptive fusion.

Fig. 10 illustrates performance differences among VMD-LSTM-SVM, VMD-LSTM, LSTM-SVM, LSTM, and SVM across various metrics. VMD-LSTM-SVM values cluster near the center (low values) on MAE, MSE, RMSE, and MAPE axes while approaching the perimeter (high value) on the R^2 axis, forming the smallest enclosed area and indicating optimal overall performance. In contrast, LSTM values

deviate furthest from the center across all metrics, creating the largest enclosed area and demonstrating the weakest performance with insufficient fitting capability. VMD-LSTM, LSTM-SVM, and SVM exhibit intermediate performance, with VMD-LSTM slightly outperforming LSTM-SVM in MAE and RMSE while achieving relatively higher R^2, and LSTM-SVM showing marginal advantage in MSE. These results confirm VMD-LSTM-SVM's comprehensive superiority, particularly in error control and fitting accuracy.

Overall, the radar-chart comparison confirms that the proposed VMD-LSTM-SVM framework achieves the most balanced performance across all metrics, with clear advantages over both the simpler standalone baselines and the intermediate hybrid comparison models.

In addition to prediction accuracy, the computational efficiency of the proposed framework is also acceptable for practical daily-scale seepage monitoring. The case study involves 998 daily samples, which keeps the overall data volume moderate. Although the VMD-LSTM-SVM framework is more computationally demanding than a single standalone model due to the decomposition step and multiple LSTM branches, its computational burden remains manageable because VMD decomposition and model training can be performed offline. Moreover, the use of a linear-kernel SVM helps maintain high regression efficiency, and the prediction stage after training is relatively lightweight. Therefore, the proposed framework is suitable for engineering scenarios in which seepage data are updated periodically rather than at extremely high frequency.

3.3 Model Prediction Result Interpretation

This section applies SHAP analysis to the VMD-LSTM-SVM framework to interpret the seepage discharge prediction results. Considering the heterogeneous structure of the model, Deep SHAP is employed for the VMD-LSTM branch and Kernel SHAP is employed for the SVM branch [27]. To ensure that the interpretation remains consistent with the prediction mechanism, the final SHAP explanation is constructed according to the same ensemble rule used for prediction. Specifically,

$$\phi_j^{\text{final}} = w_{\text{LSTM}}\phi_j^{\text{LSTM}} + w_{\text{SVM}}\phi_j^{\text{SVM}} \tag{21}$$

when weighted fusion is used; otherwise, ϕ_j^{final} is taken from the selected branch. Therefore, the SHAP results presented below correspond to the final integrated interpretation of the ensemble framework rather than to either branch alone. Unless otherwise stated, the SHAP visualizations reported in this section are based on the final integrated SHAP values of the ensemble framework.

In the SHAP feature-importance scatter plot, feature importance, feature effects, and SHAP value distributions are integrated to comprehensively demonstrate how each feature influences VMD-LSTM-SVM model predictions. The analyzed features include the current reservoir water level (wl), its lagged values (wl_lag1, wl_lag2, wl_lag3), and lagged seepage values (sp_lag1, sp_lag2, sp_lag3).

As shown in Fig. 11, current reservoir water level demonstrates the most significant contribution to seepage predictions, indicating that it is the dominant predictor in the present model. Notably, water-level lag features (wl_lag) also exhibit substantial influence, while seepage-discharge lag features show relatively minor impact, suggesting that the model gives greater weight to water-level dynamics than to seepage-history information. These findings are broadly consistent with engineering understanding of seepage behavior and therefore support the physical plausibility of the model interpretation, rather than constituting direct verification of the underlying seepage mechanisms.

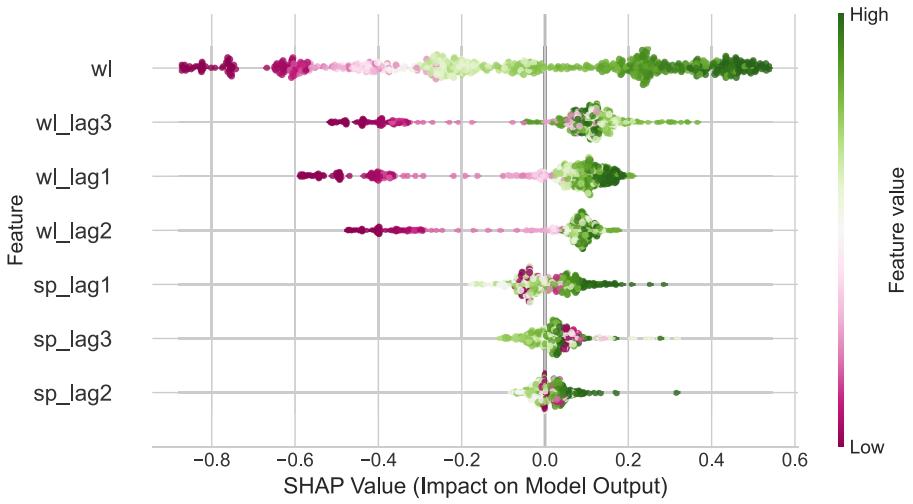

Figure 11: SHAP summary plot for the VMD-LSTM-SVM framework.

To quantitatively evaluate which features are most important for seepage discharge prediction, the average absolute SHAP value of each feature was calculated. Fig. 12, based on the VMD-LSTM-SVM model, ranks the features by overall importance. The bar chart clearly presents the contributions of the features to model predictions, with bar lengths representing normalized average SHAP values and features arranged in descending order of importance, thereby reflecting their impact on seepage discharge predictions.

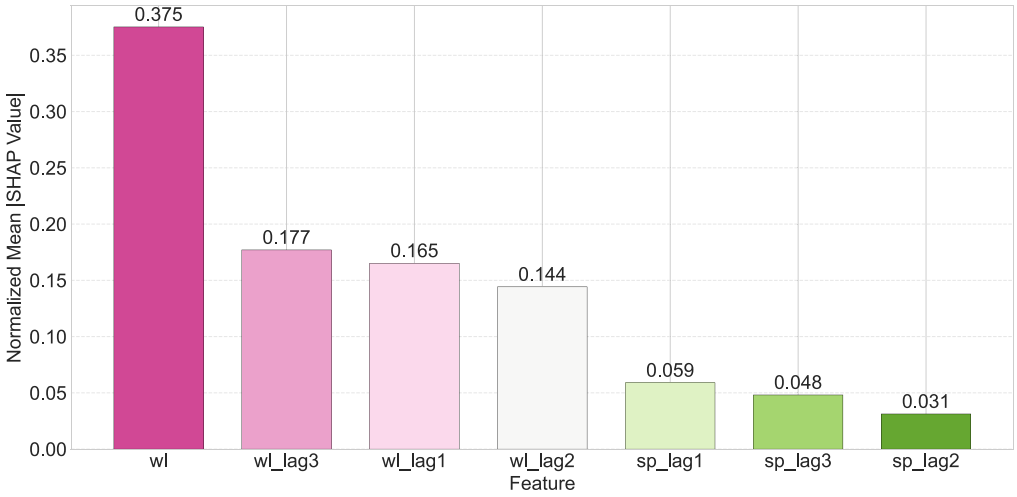

Figure 12: SHAP feature-importance bar plot for the VMD-LSTM-SVM framework.

Fig. 12 presents the average SHAP values for each feature in the VMD–LSTM–SVM model, quantifying their influence on seepage-discharge predictions. The reservoir water level (wl) shows the largest contribution, with an average SHAP value of 0.375, indicating a strong and direct effect of current hydrological conditions on seepage dynamics. Lagged water-level terms are also influential: wl_lag3 = 0.177, wl_lag1 = 0.165, and wl_lag2 = 0.144, suggesting that historical water levels continue to affect seepage, though their influence is weaker than that of the current level. By contrast, lagged seepage terms contribute less (sp_lag1 = 0.059, sp_lag3 = 0.048, sp_lag2 = 0.031). Overall, the model depends more on water-level-related variables than on past seepage values.

Fig. 13 presents the SHAP heatmap across samples, where the horizontal axis represents sample points, the vertical axis lists input features (e.g., wl_lag1, wl_lag2), and color intensity reflects the magnitude and direction of feature contributions to the predictions. This heatmap enables intuitive identification of key features and their influence patterns on predictions, providing crucial evidence for understanding model decision mechanisms.

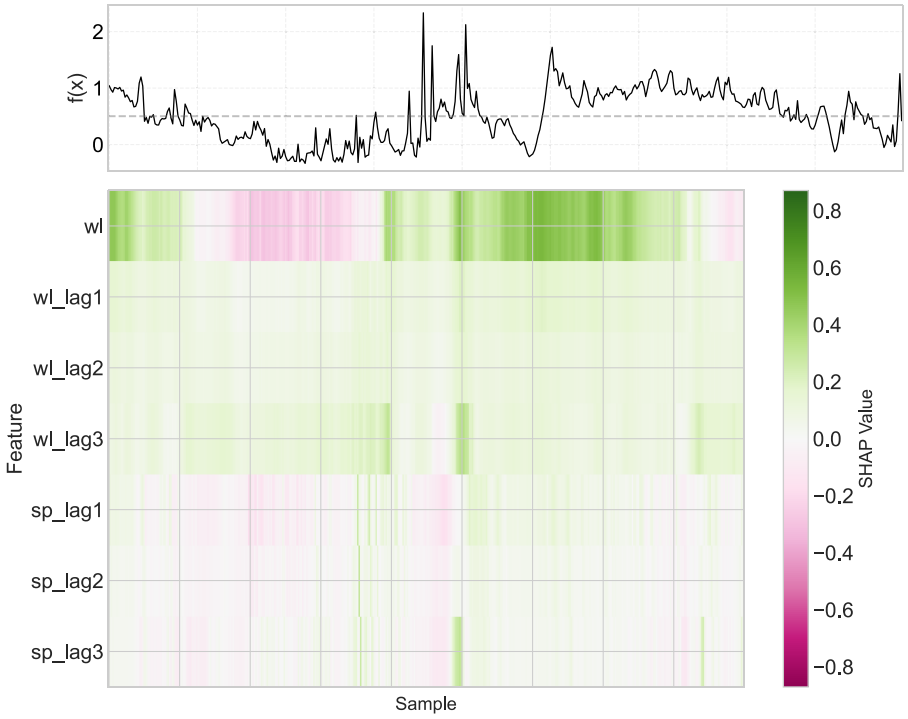

Figure 13: SHAP heatmap across samples for the VMD-LSTM-SVM framework.

Fig. 13 illustrates the VMD-LSTM-SVM model's SHAP heatmap on the training set, revealing each feature's contribution to seepage discharge predictions. The vertical axis lists features including wl, wl_lag1–3, and sp_lag1–3, while the horizontal axis represents data samples. Colors ranging from red to green (−0.8 to 0.8) indicate the negative or positive influence of features on predictions. The heatmap shows that reservoir water level exhibits deep green across multiple samples, indicating a substantial positive contribution to seepage predictions and confirming its dominant role in increasing predicted values. By contrast, the third-order seepage lag appears light red in some samples, suggesting a negative contribution in those cases. The differences in contribution patterns across features reflect how the model distributes predictive importance among temporal and hydrological inputs. These patterns provide useful interpretive support for engineering analysis and future feature selection, but should be regarded as supplementary evidence rather than direct verification of seepage-system mechanisms.

Comprehensive SHAP analysis indicates that the reservoir water level (wl) exerts the greatest influence on the model output, exhibiting the widest SHAP span (approximately −0.8 to 0.55) and the highest normalized mean SHAP value (37.5%). The lagged water-level terms provide essential temporal context, with their effects diminishing as the lag order increases, whereas the lagged seepage terms contribute only marginally. Overall, higher water levels correspond to positive SHAP contributions and lower levels to negative contributions, showing that the model relies primarily on water-level-related variables rather than past seepage values. These results substantially enhance the transparency of the ensemble model and mitigate

its "black-box" character. At the same time, the SHAP analysis should be interpreted as revealing model-based feature-contribution patterns rather than as independently establishing the full physical mechanisms of the seepage system.

Although the current SHAP analysis identifies reservoir water level and its lagged terms as the dominant predictors among the variables considered in this study, other environmental and operational factors may also influence seepage behavior in practical engineering settings. Environmental variables such as rainfall and temperature may affect infiltration conditions and material permeability, while operational factors such as reservoir regulation patterns, drainage performance, and long-term material deterioration may alter seepage pathways and response lag. In the present case study, Fig. 4 shows no direct correlation between rainfall fluctuations and seepage discharge, suggesting that surface-runoff interference was effectively isolated by the measuring weir and that reservoir water level was the dominant driver within this dataset. Nevertheless, the potential influence of additional environmental or operational variables should not be excluded for other dams or under different hydrogeological and operational conditions.

3.4 Discussion and Practical Implications

Although the proposed VMD-LSTM-SVM framework was validated using a single earth-rock dam case, its modeling logic is not limited to this specific project. The framework is built on several relatively general characteristics of seepage monitoring data, including non-stationarity, multi-scale temporal variation, lagged hydraulic response, and the need for interpretable prediction. Therefore, the method is expected to have potential applicability to other dam types and engineering settings where similar seepage-monitoring characteristics are present. However, the degree of transferability may still depend on factors such as dam type, foundation conditions, material zoning, drainage configuration, and the local hydrogeological environment. Accordingly, when applying the framework to other dams or geological conditions, site-specific recalibration of decomposition parameters, model hyperparameters, and input-variable selection may be necessary. Broader validation using data from multiple dams under different geological and operational conditions will be an important direction for future work.

In addition to the benchmark models considered in this study, broader comparisons with other machine learning frameworks may provide further insight into the relative advantages of the proposed method. For example, gradient boosting models may offer strong tabular regression performance, transformer-based time-series models may provide a more flexible mechanism for capturing long-range temporal dependencies, and Gaussian process regression may be useful for uncertainty-aware prediction in small-sample settings. Although these approaches were not included in the present study in order to maintain a focused validation framework, they represent meaningful directions for future benchmarking and could help further evaluate the applicability, robustness, and interpretability of the proposed VMD-LSTM-SVM framework.

In the present study, model interpretability is mainly evaluated through the SHAP framework, which provides a consistent quantitative explanation of feature contributions in the proposed ensemble model. Nevertheless, complementary interpretability techniques may provide additional validation of the observed feature rankings. For example, permutation importance could be used in future work as an auxiliary global interpretation tool to examine whether the dominant variables identified by SHAP remain stable under feature perturbation. Such cross-validation across different interpretability methods may further strengthen the robustness and credibility of feature-attribution results in seepage-monitoring applications.

From a practical deployment perspective, the proposed framework is intended for short-term operational forecasting in dam monitoring systems where seepage discharge and reservoir water level records are continuously updated. As with other time-series forecasting models, the present framework relies on recent historical observations as input and is therefore not intended for long-horizon extrapolation without

newly acquired monitoring data. In practical applications, the model can be embedded into a real-time monitoring workflow, in which new observations are regularly incorporated for input-window updating and short-term forecast generation. When sufficient new data accumulate or when monitoring conditions change, periodic recalibration or model retraining may also be needed to maintain forecasting reliability. Under such a deployment mode, the framework may serve as an auxiliary tool for online trend monitoring, anomaly screening, and early warning assistance, rather than as a replacement for engineering judgment.

Sensitivity analysis may also provide a useful complement to the present interpretation framework. While SHAP identifies the relative contribution of each input variable within the trained model, sensitivity analysis could further quantify how perturbations in key inputs affect the predicted seepage discharge. In particular, such analysis may help evaluate the response stability of the model to variations in hydraulic, environmental, or operational factors and provide additional support for interpreting the practical importance of different inputs. This will be a meaningful direction for future work.

Beyond short-term forecasting, the proposed framework may also support anomaly screening and early warning by comparing predicted seepage trends with newly observed monitoring data and identifying persistent deviations from expected behavior. From a methodological perspective, a further extension would be to incorporate physical constraints into the learning process, for example by combining data-driven prediction with governing relationships derived from seepage mechanics or numerical solvers. In this regard, physics-informed neural networks (PINNs) may provide a promising direction for improving physical consistency, especially when larger datasets from multiple dams become available.

4 Conclusion

Building upon existing seepage prediction model research, this study proposes an integrated "decomposition-parallel modeling-dynamic fusion-interpretability" VMD-LSTM-SVM hybrid interpretable model. Through validation with reservoir seepage data from Yunnan Province, the following conclusions are drawn:

(1) The VMD-LSTM-SVM model effectively extracts multi-scale features from seepage sequences through VMD decomposition (yielding 7 IMFs and 1 residual component), with LSTM networks precisely modeling temporal dependencies of each component and SVM integration significantly enhancing prediction stability. Empirical results demonstrate that the model outperforms all benchmark models (VMD-LSTM, LSTM-SVM, LSTM, and SVM) across all metrics. Specifically, MAE (0.0124 L/s), RMSE (0.0198 L/s), and MAPE (8.75%) are reduced by 62.65%, 55.70%, and 30.22%, respectively, compared to the best-performing baseline model (VMD-LSTM), while R^2 reaches 0.9811, validating the innovative value of multi-method coupling.

(2) Systematic performance analysis elucidates the contribution of each model component to overall prediction enhancement. The VMD preprocessing stage proves instrumental in handling non-stationary characteristics, as evidenced by VMD-LSTM achieving 20.67% higher R^2 compared to standalone LSTM. The incorporation of SVM demonstrates substantial improvements in model robustness, with the LSTM-SVM configuration reducing MAE and RMSE by 40.38% and 44.81%, respectively, relative to LSTM alone. Most significantly, the complete integrated framework leverages complementary strengths of temporal decomposition, sequence modeling, and regression analysis to achieve prediction-error reductions exceeding 55.70% compared to suboptimal alternatives, underscoring the effectiveness of the proposed ensemble architecture.

(3) SHAP interpretability analysis identifies reservoir water level as the most influential feature (37.5% contribution), indicating that water-level-related variables play a dominant role in the model's predictions.

This result enhances the interpretability of the proposed framework and is broadly consistent with engineering understanding of seepage behavior, although it should not be interpreted as direct verification of the underlying seepage mechanisms. The model's prediction accuracy meets the Class I requirements specified in SL/T 551-2024 for seepage monitoring, demonstrating practical engineering value.

The proposed framework achieves a practical balance among prediction accuracy, model robustness, and interpretability, which are critical requirements for operational dam safety monitoring. In addition, its computational burden remains manageable for periodic engineering monitoring applications, since model training can be performed offline and operational prediction after deployment is relatively efficient. Future research will focus on extending the framework with broader environmental and operational variables, validating it across multiple dams under different structural and geological conditions, and enhancing its applicability through cross-dam transfer, broader benchmarking, physically informed modeling, and long-term real-time updating.

Acknowledgement: Not applicable.

Funding Statement: This work was supported by the National Natural Science Foundation of China (Grant Nos. 52069029 and 52369026), the Belt and Road Special Foundation of the National Key Laboratory of Water Disaster Prevention (Grant No. 2023490411), the Yunnan Agricultural Basic Research Joint Special General Project (Grant Nos. 202501BD070001-060 and 202401BD070001-071), the Yunnan Key Laboratory of Water Security Open Project (Grant No. 20254916CE340051) and the Youth Talent Project of the "Xingdian Talent Support Plan" in Yunnan Province (Grant No. XDYC-QNRC-2023-0412).

Author Contributions: Menghua Li: conceptualization, methodology, experiments, data analysis, and original draft preparation. Bin Ou: supervision, methodological guidance, and critical revision of the manuscript. Jiahao Li: experiments and data collection. Sitong Jin: numerical simulations and data processing. Yanming Zhang: validation, visualization, and assistance with data analysis. Shuyan Fu: overall supervision, project administration, funding acquisition, and critical review and editing of the manuscript. All authors reviewed and approved the final version of the manuscript.

Availability of Data and Materials: The authors confirm that the data supporting the findings of this study are available within the article. Additional data are available from the Corresponding Author, Shuyan Fu, upon reasonable request.

Ethics Approval: Not applicable.

Conflicts of Interest: The authors declare no conflicts of interest.

References

1. ICOLD Committee on Dam Safety. ICOLD incident database bulletin 99 update: statistical analysis of dam failures. International Commission on Large Dams (ICOLD); 2025. Bulletin No. 99. [cited 2026 Jan 1]. Available from: https://www.icoldchile.cl/boletines/188.pdf.
2. Foster M, Fell R, Spannagle M. The statistics of embankment dam failures and accidents. Can Geotech J. 2000;37(5):1000–24. doi:10.1139/t00-030.
3. Fell R, Wan CF, Cyganiewicz J, Foster M. Time for development of internal erosion and piping in embankment dams. J Geotech Geoenviron Eng. 2003;129(4):307–14. doi:10.1061/(asce)1090-0241(2003)129:4(307).
4. Yang L, Su H, Wen Z. Improved PLS and PSO methods-based back analysis for elastic modulus of dam. Adv Eng Softw. 2019;131(1):205–16. doi:10.1016/j.advengsoft.2019.02.005.
5. Tu J, Yi J, Xiao L, Gao Q, Zhang T. A physics-informed deep learning approach using different free surface approximation strategies for steady seepage in dams. Water. 2026;18(9):1016. doi:10.3390/w18091016.

6. Huang TH, Yang YS, Yeh HF. A novel bimodal hydro-mechanical coupling model for evaluating rainfall-induced unsaturated slope stability. Geosciences. 2025;15(7):265. doi:10.3390/geosciences15070265.
7. Wang L, Li Z, Ye F, Liu T. A probability model for short-term streamflow prediction based on multi-resolution data. Water Resour Manag. 2023;37(14):5601–18. doi:10.1007/s11269-023-03620-y.
8. Kratzert F, Klotz D, Brenner C, Schulz K, Herrnegger M. Rainfall-runoff modelling using long short-term memory (LSTM) networks. Hydrol Earth Syst Sci. 2018;22(11):6005–22.
9. Tinoco J, Correia AG, Cortez P. Support vector machines applied to uniaxial compressive strength prediction of jet grouting columns. Comput Geotech. 2014;55:132–40.
10. Kang F, Li J, Zhao S, Wang Y. Structural health monitoring of concrete dams using long-term air temperature for thermal effect simulation. Eng Struct. 2019;180(8):642–53. doi:10.1016/j.engstruct.2018.11.065.
11. Fatehi-Nobarian B, Fard Moradinia S. Wavelet–ANN hybrid model evaluation in seepage prediction in nonhomogeneous earthen dams. Water Pract Technol. 2024;19(7):2492–511. doi:10.2166/wpt.2024.152.
12. Liu B, Cen W, Zheng C, Li D, Wang L. A combined optimization prediction model for earth-rock dam seepage pressure using multi-machine learning fusion with decomposition data-driven. Expert Syst Appl. 2024;242(10):122798. doi:10.1016/j.eswa.2023.122798.
13. Dragomiretskiy K, Zosso D. Variational mode decomposition. IEEE Trans Signal Process. 2013;62(3):531–44.
14. Parsaie A, Ghasemlounia R, Gharehbaghi A, Haghiabi AH, Chadee AA, Nou MRG. Novel hybrid intelligence predictive model based on successive variational mode decomposition algorithm for monthly runoff series. J Hydrol. 2024;634(9):131041. doi:10.1016/j.jhydrol.2024.131041.
15. Ma YR, Yang J, Li H, Liao H, Feng YX. Runoff prediction based on a VMD-LSTM model considering the decomposition error. J Phys Conf Ser. 2023;2491(1):012017. doi:10.1088/1742-6596/2491/1/012017.
16. Li X, Wen Z, Su H. An approach using random forest intelligent algorithm to construct a monitoring model for dam safety. Eng Comput. 2021;37(1):39–56. doi:10.1007/s00366-019-00806-0.
17. Carvalho DV, Pereira EM, Cardoso JS. Machine learning interpretability: a survey on methods and metrics. Electronics. 2019;8(8):832.
18. Lundberg SM, Lee SI. A unified approach to interpreting model predictions. Adv Neural Inf Process Syst. 2017;30:4768–77.
19. Yu HL, Wang XL, Ren BY, Zheng MW, Wu GH, Zhu KX. IAO-XGBoost ensemble learning model for seepage behavior analysis of earth-rock dam and interpretation of prediction results. Shuili Xuebao. 2023;54(10):1195–209. (In Chinese).
20. Hu J, Su H. Forecasting and analysis of deformation in hydraulic structures. Hydro-Sci Eng. 2024;(2):125–34. (In Chinese).
21. Zhang X, Xia Y, Zhang C, Liu B, Wang C, Fang H, et al. A prediction model for dyke-dam piping based on data augmentation and interpretable ensemble learning. Eng Fail Anal. 2025;182(3):110174. doi:10.1016/j.engfailanal.2025.110174.
22. Li F, Zhang B, Verma S, Marfurt KJ. Seismic signal denoising using thresholded variational mode decomposition. Explor Geophys. 2018;49(4):450–61. doi:10.1071/eg17004.
23. Krichen M, Mihoub A. Long short-term memory networks: a comprehensive survey. AI. 2025;6(9):215. doi:10.3390/ai6090215.
24. Vapnik V, Golowich S, Smola A. Support vector method for function approximation, regression estimation and signal processing. Adv Neural Inf Process Syst. 1996;9:281–7.
25. Zuo G, Luo J, Wang N, Lian Y, He X. Decomposition ensemble model based on variational mode decomposition and long short-term memory for streamflow forecasting. J Hydrol. 2020;585(3–4):124776. doi:10.1016/j.jhydrol.2020.124776.
26. Ou B, Zhang C, Xu B, Fu S, Liu Z, Wang K. Innovative approach to dam deformation analysis: integration of VMD, fractal theory, and WOA-DELM. Struct Control Health Monit. 2024;2024(1):1710019.
27. Mubarak H, Stegen S, Bai F, Abdellatif A, Sanjari MJ. Enhancing interpretability in power management: a time-encoded household energy forecasting using hybrid deep learning model. Energy Convers Manag. 2024;315:118795.